Chapter 7

Well logs as tensorial quantities

In this chapter I discuss my application of tensor fields to an area where generally only scalar fields have been used to improve the agreement between parameters measured in different types of experiments. The transformation of measured scalar quantities in well logs to tensors allows for an improved description of the medium. The primary example in the chapter demonstrates the prediction of surface seismic velocities from well logs.

Observations based on measurements taken on different scales may not agree. However, an equivalent-medium approach can link measurements carried out at different scales. I have applied high-frequency (Dix) and low-frequency (Schoenberg&Muir) averages to a well log. This study compares the results of a conventional velocity analysis of surface seismic data.

In every physical experiment of finite size and duration carried out in nature, the measurement takes place over a certain scale. The actual value of the scale is determined by the discrete sampling of a natural phenomenon. For surface seismic measurements, the time scale is determined by the length of recording time, and the frequency scale by the temporal sampling interval. Both scales are related; in effect, they are exhibiting duality properties and serve as an upper limit of observable scales. What scale is actually observed depends on the experiment itself; for example, one determining factor is the frequency content of a seismic source radiating energy into the subsurface. Scale dimensions can vary to a limited degree, depending on the type of seismic experiment. Given that the subsurface structure can be heterogeneous on any scale, the spatial correlation of material properties is directly related to the scale of heterogeneities. When elastic waves propagate in the subsurface, the subsurface velocity and the given temporal frequency determine the

spatial wave number locally for any given point in space. The equation describing the wave propagation couples spatial and temporal resolution.

Let us imagine a high-frequency seismic surface source for which frequency and bandwidth go to infinity and for which the spatial sampling interval shrinks infinitely. In such a case, reflected energy could be recorded and resolved from infinitesimal scale obstacles. Lowering the frequency content of the source and increasing spatial sampling intervals only enables us to record wave propagation effects (reflection, diffraction) at a larger scale. Thus, we can only hope to resolve properly obstacles (layers, diffractors) that are of the order of that minimum/dominant wavelength. However, if there are material discontinuities much smaller in scale than our minimum/dominant wavelength, then a wave through a medium will "feel" some average effect. Folstad et al. (1992) made synthetic comparisons of fine- and large-scale wave propagation effects using a Backus averaging of elastic constants. Thus, for a given finite resolution, we can only measure the properties of the equivalent medium at that scale. Small-scale variations still influence effects at a larger scale, but we only understand them in some averaged sense. In this chapter, I introduce one application of equivalent medium theory in the form of homogeneous overburden replacement. Using such a group-theoretical approach, I find normal moveout (NMO), or focusing, velocities by calculating an anisotropic elastic replacement medium and subsequently approximating small offsets along the vertical and horizontal axes. The sections that follow compare this low-frequency with a high-frequency Dix rms velocity calculation.

7.1 The effective medium

Dix defines an average medium in the infinite frequency/bandwidth limit, thus ending up with a paraxial approximation, the rms velocity. His exposition is based on scalar-wave traveltimes and is purely kinematic. We can call this a *ray average*, because rays see well-defined interfaces in the medium. Schoenberg and Muir (Schoenberg and Muir, 1989), on the other hand, operate within the very low-frequency (long wavelength) spectrum of observations. Within this range, their approach lends itself to anisotropic media and even dipping interfaces. Their theory can be cast in terms of an equivalent medium scheme that preserves well-defined properties. It extends beyond kinematics. I call this a *wave average*, because it is more closely related to basic elastic quantities, namely stress and

strain. In reality, observations lie in a frequency regime that might be closer to one or the other frequency limit. In the following sections I compare both schemes.

7.2 Typical seismic experiment scales

Seismic measurements at different scales have different objectives and may result in different observations. However, the measured property still provides information about a unique medium. Thus, in theory, it should be possible to relate differently scaled measurements to one another. In the past, there seems to have been a lack of success in this regard. Typically, NMO velocities from surface seismic data do not agree well with sonic logs. This has long been a recognized problem. For example, in common empirical approaches, check shots are used to stretch the seismic log to a surface seismic scale, but lack a rigorous physical explanation. However, equivalent medium schemes suggest ways to relate measurements carried out at different scales. Moreover, one knows exactly which quantities are preserved in the rescaling process. In this particular application, I assume that velocity does not vary too drastically over the given frequency interval, so that velocity dispersion will not be accounted for.

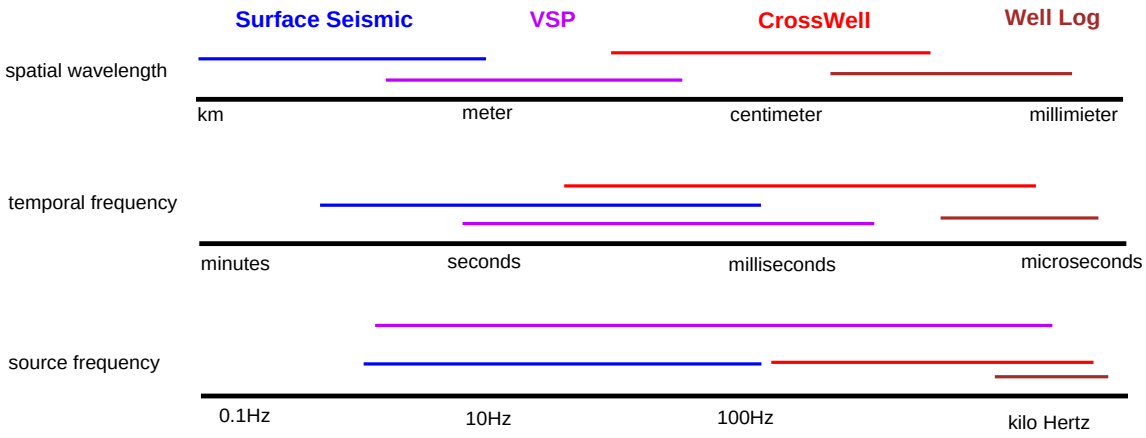

FIG. 7.1. Schematic display of different types of measurements with various spatial and temporal frequency. The border between experiments is not distinct; there can be a fair amount of overlap between different experiment types. tensorlog-cartoon [NR]

Surface seismic measurements

The scale length in surface seismic measurements is generally in the range of kilometers or tens of meters. In particular, for exploration applications, a typical scale length of tens/hundreds of meters is common. The temporal scale is on the order of a few seconds, while the source frequency is usually between 1-100 Hz.

Vertical seismic profiles

Vertical seismic profile (VSP) experiments, including reversed VSPs, can display a large overlap in scale with surface seismic ones. On the other hand, the spatial scale typically ranges from meters down to decimeters. Depending on the type of source, surface or bore hole, the temporal frequency scale ranges from surface seismic values down to crosswell values.

Crosswell measurements

In Crosswell measurements, scale overlaps are likely with VSP but not with surface seismics. On the other hand, overlap with well log values is also possible. This behavior holds for temporal and spatial frequencies as well because distances are generally smaller than for the VSP experiment. The usable source frequency can vary extensively.

Well log measurements

Among the kinds of measurements included in this study, well logs occupy the lowest spectrum of scales. Cross well measurements can overlap with well log measurements, but it is very unlikely that there is overlap with any of the other considered experiments (VSP and surface seismic measurements). Obviously, then, the most challenging task is to relate well log to surface seismic measurements. Figures 7.2 and 7.3 show stacking velocities and sonic logs obtained at the same surface location that clearly demonstrate how experimental scale differences can lead to quite different results in resolution and values, although both experiments measure the same medium. This discrepancy is especially problematic when comparing borehole sonic logs and surface seismic velocity estimations.

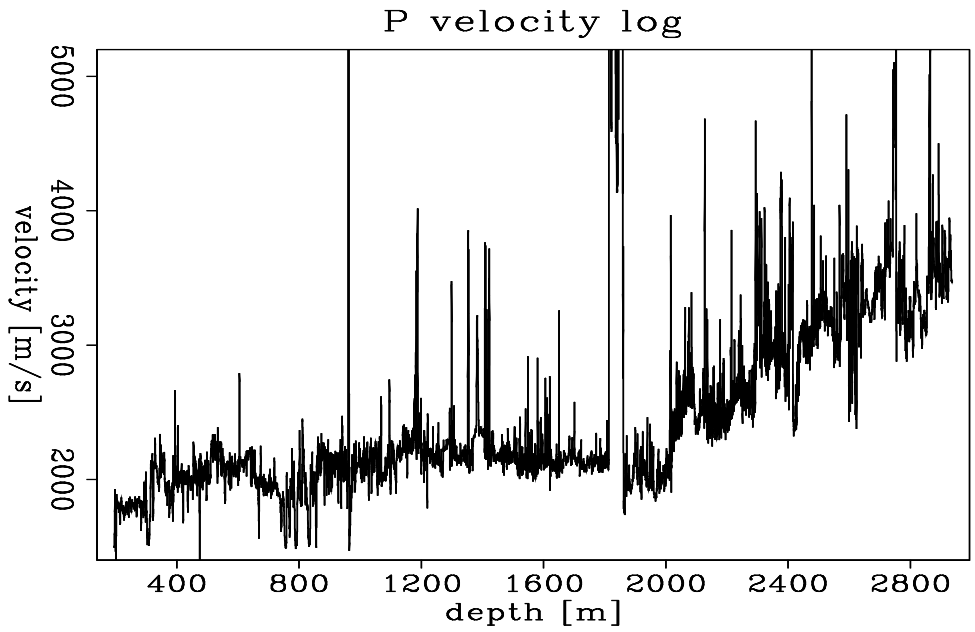

FIG. 7.2. A well log, showing the P-wave sonic velocity with depth. tensorlog-velp [CR]

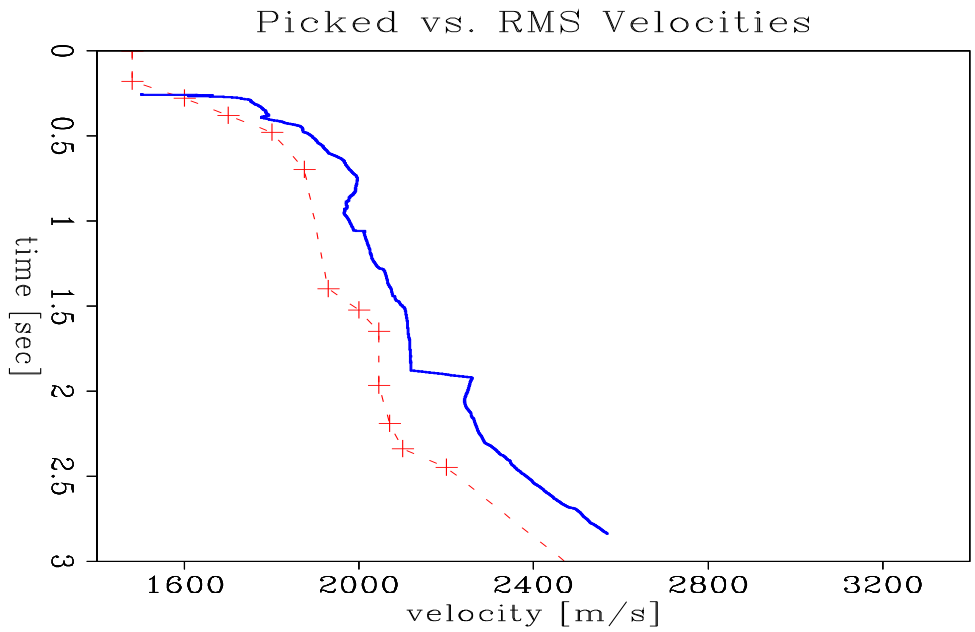

FIG. 7.3. Comparison of the stacking velocity (dashed line) picked from a conventional velocity analysis and the rms velocity (solid line) calculated from the original P-wave sonic log in Figure 7.2. tensorlog-pickrms [CR]

7.3 Assumptions of equivalent medium averaging

All averaging schemes discussed here are based on a layered earth model. The S&M approach is valid within the limits of long wavelengths, where the layer thickness is much smaller than a wavelength. This approach averages horizontal dipping layers and comes up with a homogeneous equivalent medium. It is essentially a low-frequency wave averaging scheme. Dix's method, on the other hand, applies to infinite frequency and bandwidth, and is essentially a ray averaging scheme. Obviously, surface seismic data lie between those two extremes, potentially with some bias toward the low-frequency end. The next section compares the two methodologies for obtaining average velocities.

7.4 Methodology of creating an elastic log

Given the premise that conventional sonic logs measure vertical travel time in the subsurface formation, we assume that the elastic properties of the layer are isotropic. Whether this is actually the case can only be determined by making additional measurements. On one hand, a rms velocity calculation, following Dix, uses that vertical velocity to come up with an NMO velocity. This velocity is isotropic, unless extended to anisotropy, as shown by Dellinger and Muir (1993). S&M equivalent medium averaging, on the other hand, works with hybrid matrices of stiffness and compliance. Thus, this averaging requires P-wave and S-wave velocities and density in a layer to be known. If we again assume that the layer is isotropic, these three parameters determine the elastic properties uniquely. However, when we use the S&M average, in contrast to the conventional Dix average, the resulting average layer may or may not be isotropic, and will manifest itself in differences between vertical velocity (depth mapping) and move-out velocity (NMO velocity).
Currently, P- and S-wave sonics and density measurements are more commonly recorded than they were in the past, when only P-wave sonics and density were available (Figure 7.4 shows all log information that can be possibly used by this method). If a shear wave log is not available, we need to estimate one from other auxiliary information. The examples in this paper assume a constant pressure/shear wave velocity ratio. This is clearly an erroneous assumption for the target zone, since the reservoir's Poisson ratio is different from the embedding medium.

Some well logs include a dipmeter measurement, which gives an estimate of the spatial orientation of a layer. The dip of a plane layer is one more possible parameter in the

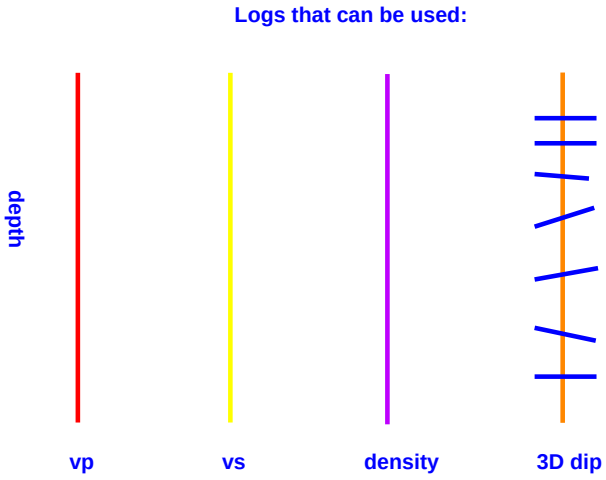

FIG. 7.4. A schematic drawing illustrates the different well log quantities that can be used to create a tensorial well log. tensorlog-quantities [NR]

S&M average. Using it ensures that the coordinate system in which the average is carried out is rotated appropriately. Moreover, since the S&M average is based on the elastic properties, it can readily incorporate any information that may be measured in the future, such as velocities at different propagation angles and orientations. Figure 7.5 illustrates the elastic log used during averaging. Employing a reasonable method of scaling well log information up to surface seismic measurements may help in constraining stacking velocities during velocity analysis at points close to a seismic line. It may also help in estimating velocities for depth mapping (in general, focusing and depth mapping velocities are not identical). In this chapter I base my analysis on stacking velocities, but the application to focusing and depth mapping is a straightforward extension.

7.5 Averaging a log

The justification for smoothing well logs using the S&M calculus is that it allows us to relate to surface seismic measurements by replacing the overburden with an equivalent homogeneous elastic medium. If a smoothing method is used to relate well logs to surface seismic measurements, the length of the smoothing filter is the crucial parameter. One choice is to smooth over the smallest possible wave number determined by the surface method. This is the shortest wavelength that appears locally when a wave is propagating through a medium. We can average over that wavelength using S&M's layer addition, with which average stress and strain components are calculated, characterizing the effective

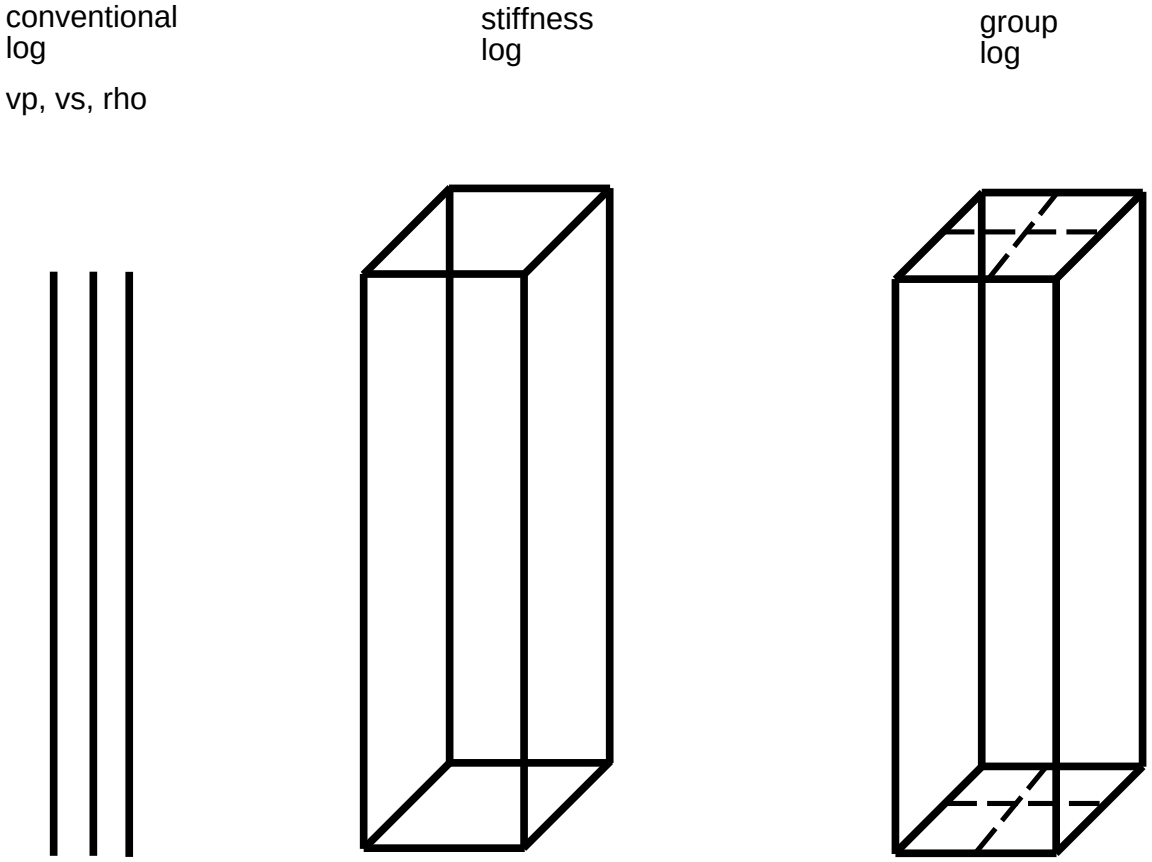

FIG. 7.5. A schematic drawing illustrates the steps in generating the elastic log. Assuming isotropy, stiffnesses can be calculated from v_p,v_s, and ρ. The S&M group transformation rearranges the stiffness log in a hybrid matrix of stiffness and compliance. The result is the group log. tensorlog-groupcartoon [NR]

medium on a larger scale. It is important to note that this method does not smooth traveltimes directly (as Dix's more or less does and as Figure 7.6 illustrates) but rather the method assumes that the measured traveltimes represent vertical traveltimes only.

Further assuming isotropic layers (this is not necessary if we have more information), the P- and S-wave sonic log and the density log specify an isotropic stiffness matrix. For each well log point in depth, these measurements are transformed into the group domain (S&M, 1990). The important point is that all the smoothing is carried out in the group domain. The following equation

$$v_p, v_s, \rho \leftrightarrow c_{ijkl} \leftrightarrow g \leftrightarrow \text{Operator} \leftrightarrow g^* \leftrightarrow v_x, v_z, v_{xnmo}, v_{znmo} \tag{7.1}$$

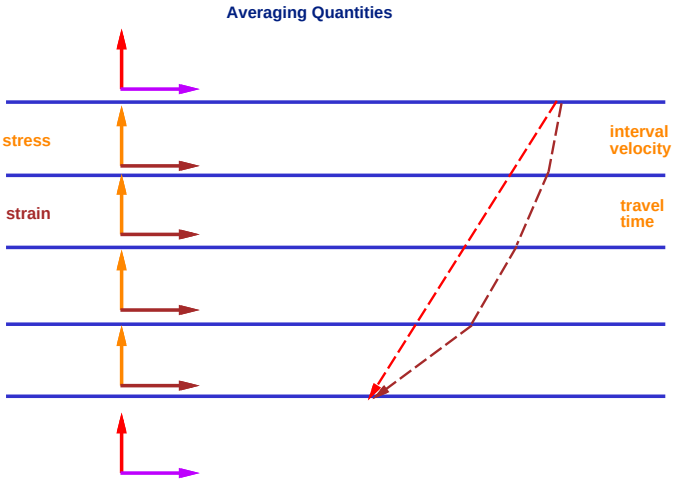

FIG. 7.6. Dix's method more or less smoothes traveltimes (velocities) directly, while the S&M equivalent medium method smoothes tensorial quantities across layer boundaries. tensorlog-veltime [NR]

schematizes the steps from a conventional log to a log that is equivalent "in some sense." In Appendix A I summarize the key equations necessary to perform computations on the left hand side of equation (7.1); in Appendix B I detail the approximation to compute the right hand side of equation (7.1). The original log is converted to elastic stiffnesses c_{ijkl}, which in turn can be transformed in S&M group domain, whose elements are g. An arbitrary operator can then be applied in the group domain. The resulting group elements g^* can be converted into quantities relating to a particular wave type and propagation direction, for example, $v_x, v_z, v_{xnmo}, v_{znmo}$. Since the S&M group transformation is a linear operation, we can apply any smoothing filter or other transform, such as the Fourier transform, in the group domain. Moreover, we can reverse all steps in equation (7.1) as long as the operator itself is reversible.

It is not readily clear what the best smoothing operator is. I chose to use a boxcar smoothing operator. After the data in the group domain are smoothed, the resulting effective medium is generally not isotropic, but instead transversely isotropic. A useful elliptic approximation, as derived by Muir (1991b) and illustrated in Figure 7.7, determines an effective NMO velocity in the smoothed medium. Figure 7.8 shows the ingredients for generating the isotropic stiffness log. The S&M group transformation is applied to the stiffness log, resulting in a group log. Using this group log $X(\zeta)$, an equivalent medium can be calculated by partially integrating all the layers up to a certain depth point in the

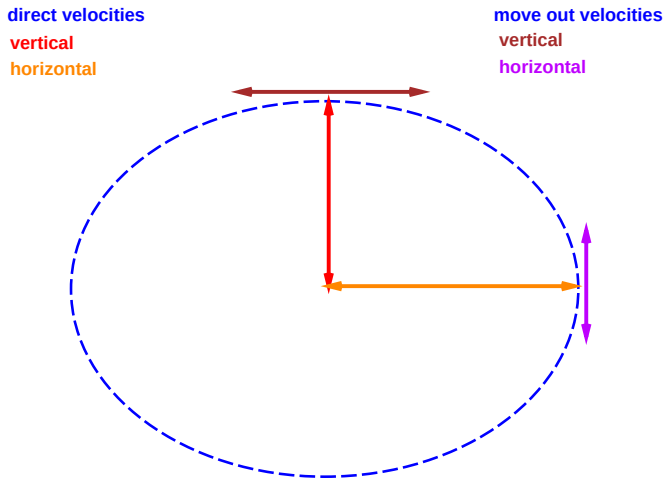

FIG. 7.7. Muir approximates the phase slowness and group velocity curves by expanding around the vertical and horizontal axes and retaining terms that include the direct propagation velocity and NMO velocity. tensorlog-veldraw [NR]

log, as given by

$$X^{equiv}(z) = \int_0^z X(\zeta) d\zeta. \tag{7.2}$$

This integration, explained in more detail in Appendix A, replaces the overburden at a specific depth point with a homogeneous equivalent medium. At the same time, it preserves all stress and strain components across layer boundaries, honoring solid-solid boundary conditions exactly. The elastic energy is conserved in this averaging process. See Nichols and Karrenbach (1990) or Hill (1983) for more details.

Figure 7.9 shows the Dix rms velocity derived using a well log and the horizontal and vertical velocities calculated using the S&M partial integration. The Dix rms velocity is the solid curve, which is nearly identical to the horizontal S&M velocity v_x. The vertical propagation velocity v_z is clearly distinct from these other two curves. It is not surprising that this partially-integrated medium is no longer isotropic. It is a well-known fact (Backus, 1962) that a sequence of thin layers produces anisotropic propagation effects for wavelengths much longer than the layering scale. Assuming that the original material was thinly-layered isotropic, the partially-integrated medium is now transverse isotropic. I only compared P velocities, since I started out with only a P sonic log and had to assume a shear wave velocity. For the result in Figure 7.9, I extracted only direct wave velocities; but by using a paraxial approximation (Dellinger et al., 1993), it was possible to extract NMO velocities. The relations in the appendix explain how in paraxial approximation around the vertical axis for TI media, moveout velocities can be obtained from elastic

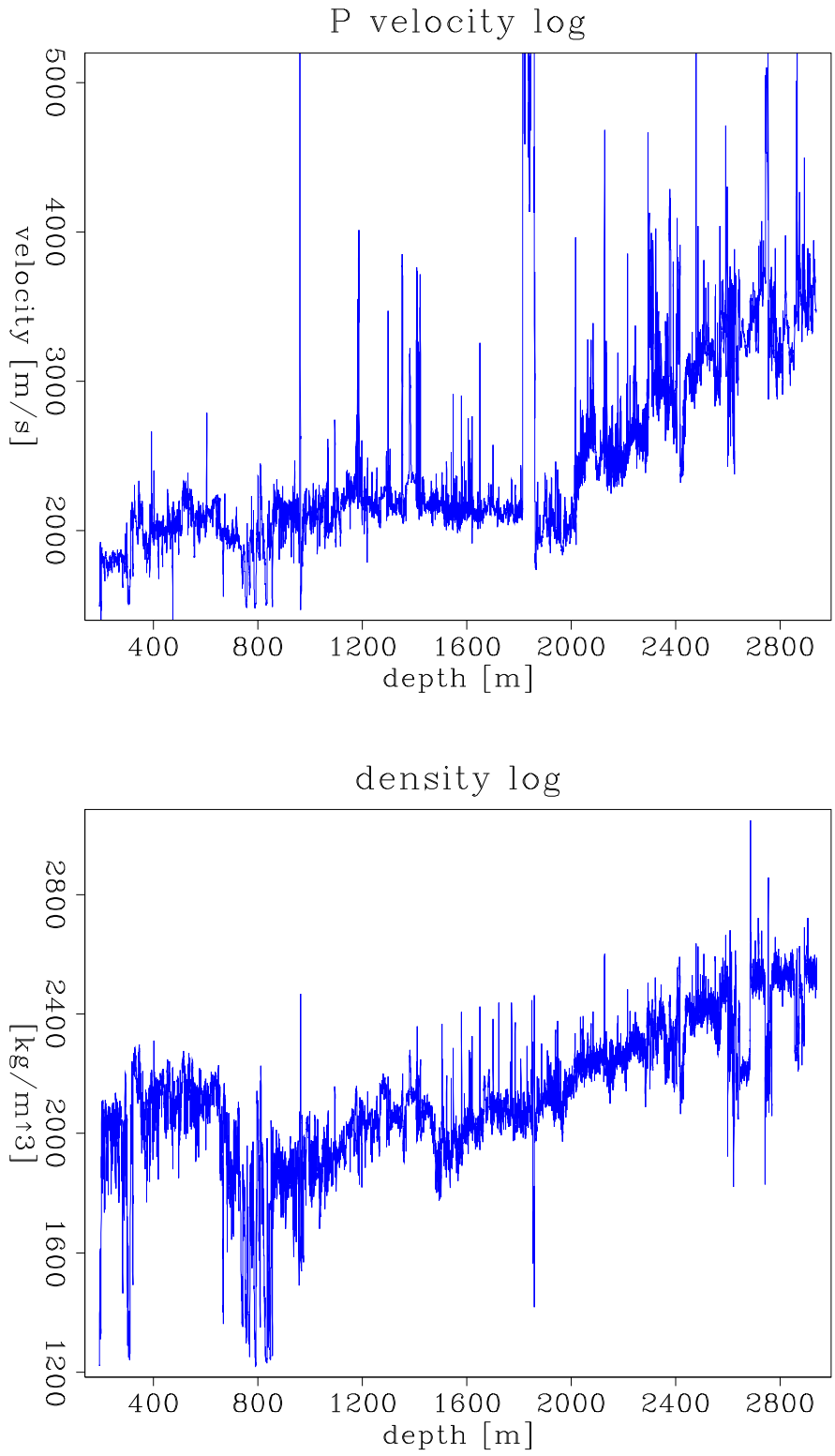

FIG. 7.8. P-wave velocity and density log measured a well site, where surface seismic data have been collected. The target zone is between 1800 and 1900 meters in depth and shows anomalous behavior in both velocity and density log. tensorlog-velprho [CR]

properties.

Figure 7.10 shows the Dix rms velocity and the wave-averaged NMO velocity. The solid curve represents the Dix rms velocity. The dashed curve indicates the horizontal NMO velocity v_{xpnmo} calculated using S&M partial integration, the dotted curve, the corresponding vertical NMO velocity v_{zpnmo}. A marine surface seismic observation measures normal moveout velocity v_{xpnmo} from a finite offset range, but leaves the vertical direct velocity ambiguous. As Figure 7.10 shows, there is only a small difference at small depth ranges, but growing disagreement at larger depth. As expected, S&M-derived curves are always lower than the Dix rms velocity. The Dix rms velocity is a high-frequency approximation satisfying Fermat's principle and thus provides us with the minimum travel time.

The crucial test that decides which averaging scheme conforms to observations better, however, is a comparison of these well-log-derived velocity curves to actual surface seismic velocity analysis data. Figure 7.11 shows a CMP gather taken at the well site. Figure 7.12 shows a semblance velocity analysis of that same gather. Overlaid are the two estimated velocity curves. The leftmost curve shows the NMO velocity derived from the S&M partially-integrated stiffness log, the rightmost the Dix rms velocity. The velocity analysis uses only the raw data with a divergence correction; no other processing is applied. The multiples appear very strongly in the semblance panel. Some primaries are visible, and the S&M-derived NMO velocity curves follow fairly closely some primary semblance peaks at times less than 2.0 seconds. The Dix rms velocity is located off the semblance peaks toward higher velocity values, except for the water bottom reflection and close arrivals. Both curves miss a primary peak at around 1.5 seconds. This peak is a reflection from a slightly dipping interface. Thus, the velocity is shifted toward higher values than predicted from a horizontal layer assumption. Below the target around 2.0 seconds, the peaks are shifted again toward higher values. Layers at that depth exhibit progressively steeper dips. The high contrast at the target zone gives rise to strong interbed multiples.

The following equations summarize the velocity relationships for matching surface seismic velocity analysis with well log observations:

$$v_{rmsp} = v_{xp} > v_{zp} \tag{7.3}$$

The direct horizontal propagation velocity v_{xp} is essentially the same velocity component as that sampled by the P-wave rms velocity. Thus, their values are nearly identical.

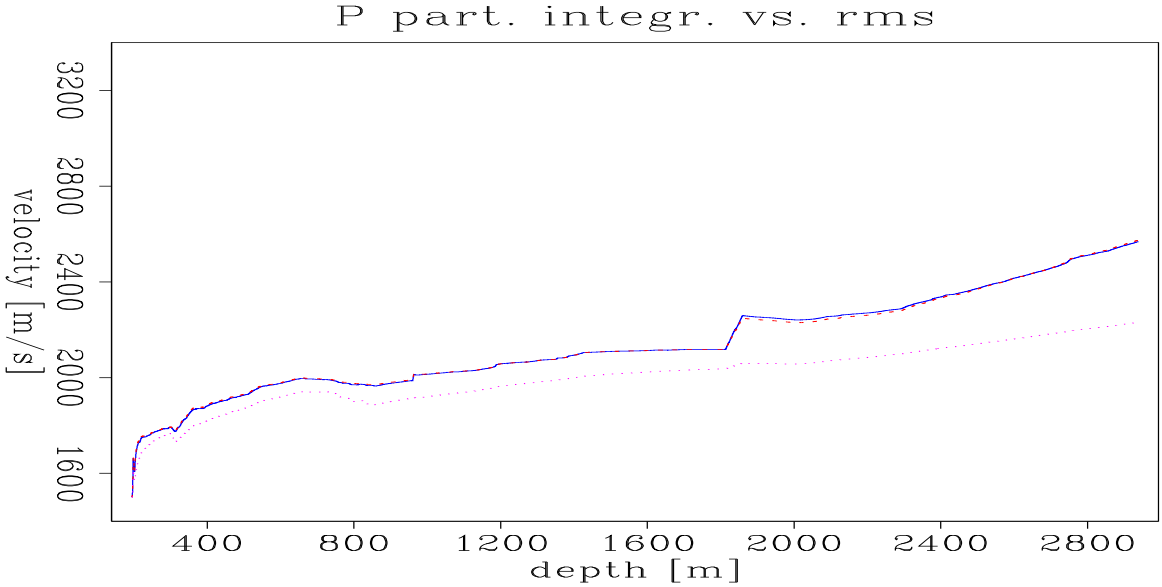

FIG. 7.9. Dix rms velocity calculated from the well log (solid line). The two other curves are the S&M partially-integrated horizontal and vertical propagation velocities (v_z = dotted, v_x = dashed). The horizontal velocity is nearly identical to the rms velocity. tensorlog-velrmsp [CR]

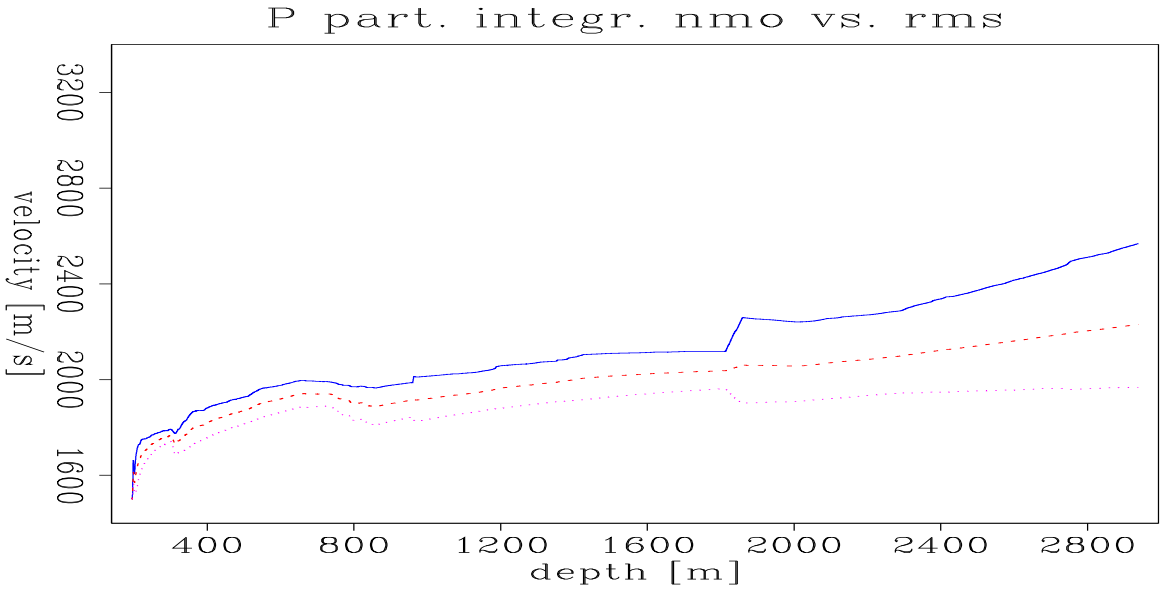

FIG. 7.10. Dix rms velocity calculated from the well log (solid line). The two other curves are the S&M partially-integrated horizontal and vertical NMO velocities (v_{zpnmo} = dotted, v_{xpnmo} = dashed). Both NMO velocities clearly differ from the rms velocity. tensorlog-velrmspnmo [CR]

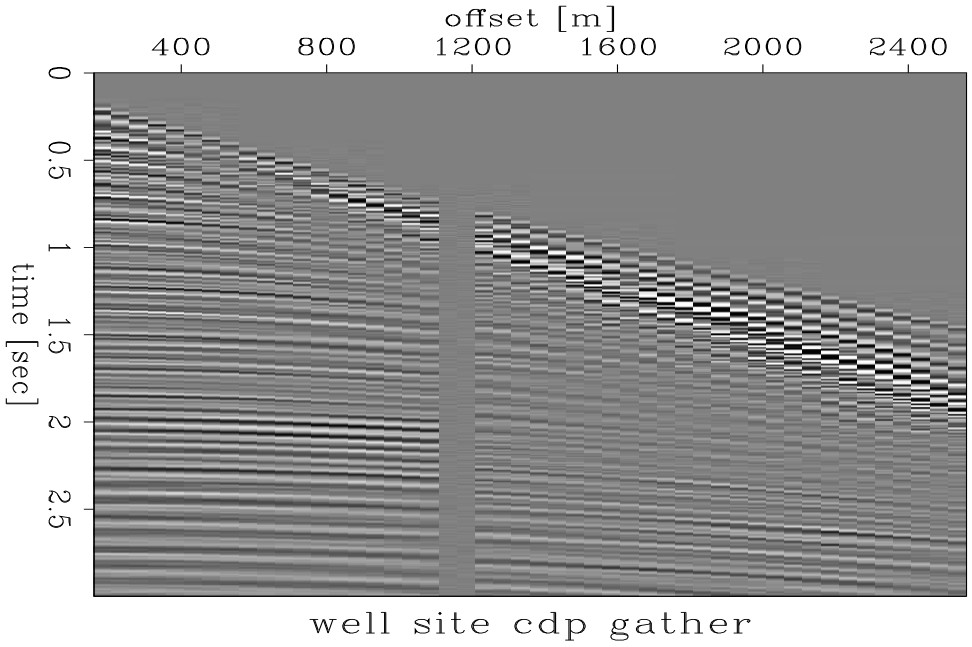

FIG. 7.11. Marine CMP gather at the well site. tensorlog-cdp641 [CR]

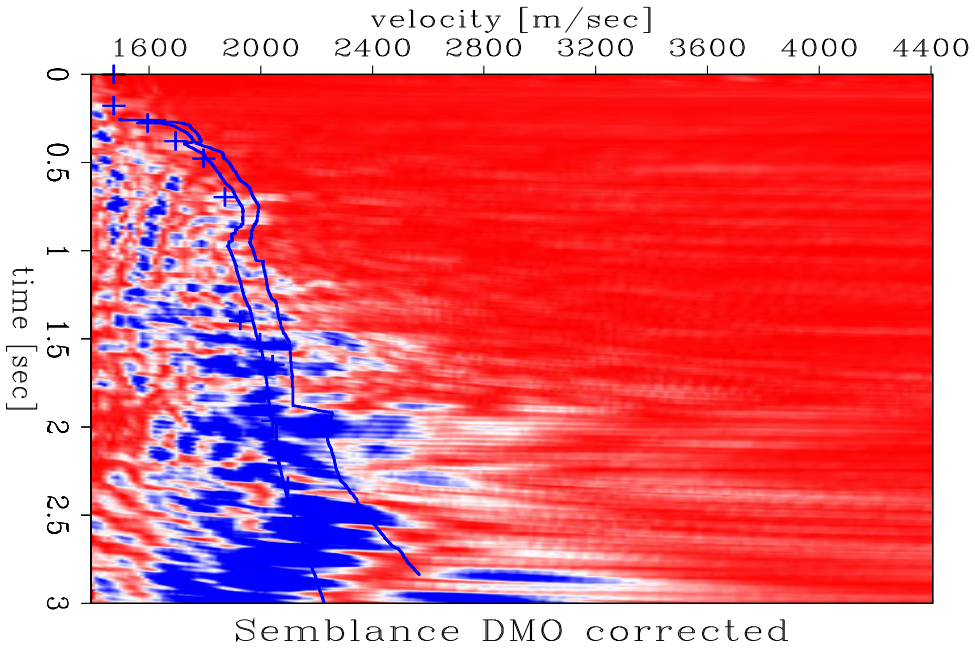

FIG. 7.12. Semblance of a 2-D DMO corrected gather with picks. The partially-integrated curve (leftmost) and rms curve (rightmost) are overlaid. tensorlog-sembdmo [CR]

The horizontal direct propagation velocity v_{xp} is parallel to the layer interfaces, while the vertical direct propagation velocity v_{zp} is perpendicular to the layering. The layering tends to lower the vertical with respect to the horizontal direct propagation velocity. The rms velocity is derived from Fermat's principle (high-frequency approximation) and thus has to fulfill the least traveltime condition. The rms velocity is therefore higher than the vertical and horizontal NMO velocities. The velocities v_{xpnmo} and v_{xznmo} are not necessarily least traveltime measurements, because they are derived from low-frequency elastic constants. Although those velocities relate to the wavefront curvature at small offsets, they include effects caused by the micro structure of the medium, such as multiple bounces (not least traveltime). The relationships between NMO velocities are

$$v_{rmsp} > v_{xpnmo} > v_{zpnmo}. \tag{7.4}$$

The relationships between direct propagation and NMO velocities are as follows:

$$v_{xp} > v_{xpnmo} \tag{7.5}$$

$$v_{zp} > v_{zpnmo} \tag{7.6}$$

$$v_{xp} > v_{zpnmo} \tag{7.7}$$

$$v_{zp} > v_{xpnmo} \tag{7.8}$$

The last relationship (7.8) relates the two most interesting quantities for surface seismic data, the direct vertical propagation velocity v_{zp} and the normal moveout velocity v_{xpnmo}. In some special cases (described in the appendix) those two quantities can be made equal, but in general they are not equal. Figure 7.13 illustrates the results I obtained using Dix rms and the S&M partial integration to relate well log measurements to surface seismic velocity analyses. As the result in the figure indicates, the velocity predicted by S&M's method is generally closer to the velocity picks. The largest difference in prediction using rms velocities is 15%, while differences between the S&M predictions are on the order of a few percent.

The previous examples comparing NMO and stacking velocities imply that the propagating wave averages those quantities over a very large wavelength. The results indicate that for velocity analysis, the wave propagation effects are better described using a low-frequency rather than a high-frequency averaging approach.

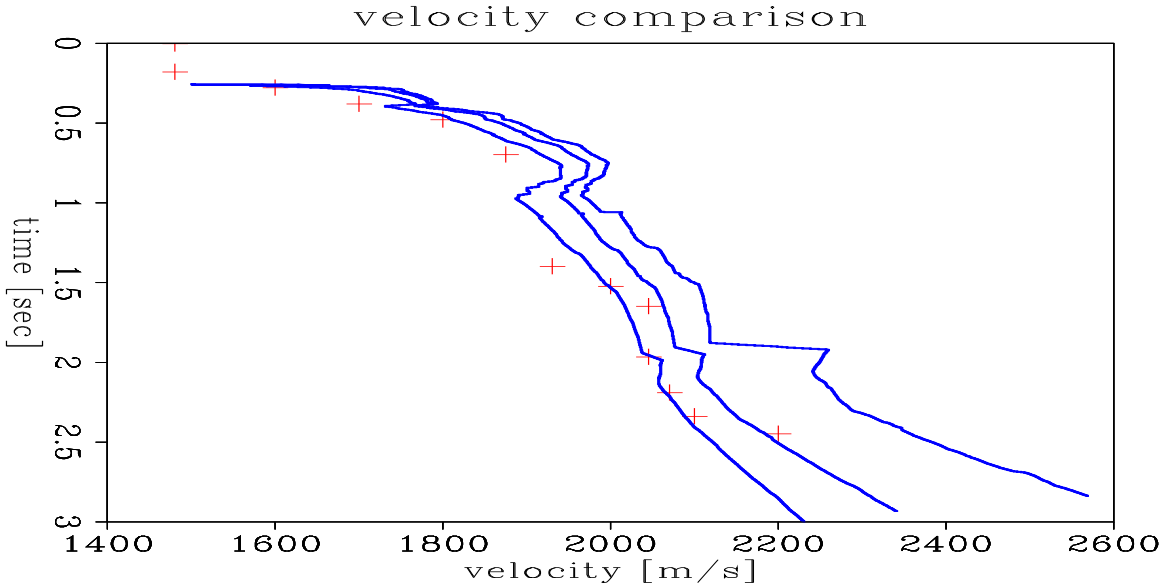

FIG. 7.13. Comparison of picks with Dix rms and S&M-predicted NMO velocities. In general, the S&M predicted velocity is closer to the velocity picks. The largest difference in prediction using rms velocities is 15%, while S&M predictions are on the order of a few percent. tensorlog-summarize [CR]

7.6 Summary

A comparison of Dix's and Schoenberg & Muir's averaging of a well log with respect to surface seismic velocity analysis reveals that both approaches replace the overburden with a homogeneous equivalent medium. However, the sense of averaging is different. Overlaying velocity analysis, Dix rms velocity, and S&M- derived velocities show that Dix rms velocity seems consistently higher (up to 15%). The S&M average produced velocities closer to the analysis picks (up to 5% deviation); at large depths, however, it was noticeably different from the velocity picks. The S&M average is consistently lower than the Dix rms average — as we would expect — since the high-frequency average is based on Fermat's principle and thus represents the minimum traveltime.

7.7 Appendix A: Converting to the group domain and back

This section shows how to convert a well log to the group domain where all the averaging takes places. I summarize key equations and techniques explained in Schoenberg and Muir (1989) and Backus (1962), and I follow the abbreviated derivation of Nichols and Karrenbach (1990).

7.7.1 From the well log to the tensor log

The well log measures p-wave velocity, s-wave velocity and density at each point in depth. I assume that the measured quantities probed an isotropic elastic medium mostly along the vertical axis and this allows me to convert directly to stiffness constants:

$$c_{33} = \rho v_p^2 \qquad \text{and} \qquad c_{44} = \rho v_s^2, \tag{A - 7.1}$$

I deduce the remaining missing stiffness values using symmetry arguments: $c_{11} = c_{22} = c_{33}$, $c_{44} = c_{55} = c_{66}$, and $c_{12} = c_{13} = c_{11} - 2 * c_{55}$. At this point, one has the complete stiffness tensor at each point in depth available.

7.7.2 From tensor log to the group domain log

To carry out equivalent medium averaging, I convert the stiffness log into the group domain. This conversion is necessary since I to replace discontinuous individual layers by their homogeneous equivalent medium by averaging over all discontinuous quantities.

The group domain for a horizontally layered earth is defined by Schoenberg and Muir (1989). The continuous stress components acting on a plane normal to the 3-axis (depth) are $\sigma_{13}, \sigma_{23}, \sigma_{33}$; the continuous strain components $\epsilon_{11},\ \epsilon_{12},\ \epsilon_{22}$ are tangential to the 3-axis. The remaining stress and strain components can be discontinuous from layer to layer. Following Nichols and Karrenbach (1990), the group domain can be derived by partitioning stress and strain vectors into continuous and discontinuous sub-vectors. The continuous parts are

$$\sigma_N \equiv \begin{pmatrix} \sigma_3 \\ \sigma_4 \\ \sigma_5 \end{pmatrix} \equiv \begin{pmatrix} \sigma_{33} \\ \sigma_{23} \\ \sigma_{13} \end{pmatrix}, \quad \epsilon_T \equiv \begin{pmatrix} \epsilon_1 \\ \epsilon_2 \\ \epsilon_6 \end{pmatrix} \equiv \begin{pmatrix} \epsilon_{11} \\ \epsilon_{22} \\ \epsilon_{12} \end{pmatrix} \tag{A - 7.2}$$

and the discontinuous parts are

$$\epsilon_N \equiv \begin{pmatrix} \epsilon_3 \\ \epsilon_4 \\ \epsilon_5 \end{pmatrix} \equiv \begin{pmatrix} \epsilon_{33} \\ \epsilon_{23} \\ \epsilon_{13} \end{pmatrix} \quad , \quad \sigma_T \equiv \begin{pmatrix} \sigma_1 \\ \sigma_2 \\ \sigma_6 \end{pmatrix} \equiv \begin{pmatrix} \sigma_{11} \\ \sigma_{22} \\ \sigma_{12} \end{pmatrix} \quad . \qquad (\mathrm{A}-7.3)$$

Consequently, one needs to adapt Hooke's law to this partitioning, such that

$$\begin{pmatrix} \sigma_T \\ \sigma_N \end{pmatrix} = \begin{pmatrix} \mathbf{C}_{TT} & \mathbf{C}_{TN} \\ \mathbf{C}_{NT} & \mathbf{C}_{NN} \end{pmatrix} \begin{pmatrix} \epsilon_T \\ \epsilon_N \end{pmatrix} = \begin{pmatrix} \mathbf{S}_{TT} & \mathbf{S}_{TN} \\ \mathbf{S}_{NT} & \mathbf{S}_{NN} \end{pmatrix} \begin{pmatrix} \sigma_T \\ \sigma_N \end{pmatrix} \qquad (\mathrm{A}-7.4)$$

These partitioned representations can be combined to relate discontinuous tensor components on the left-hand side with continuous tensor components on the right-hand sides. A new form of Hooke's law is obtained, where a hybrid (stiffness and compliance) matrix governs the constitutive equation.

$$\begin{pmatrix} \sigma_T \\ \epsilon_N \end{pmatrix} = \begin{pmatrix} {\mathbf{S}_{TT}}^{-1} & {\mathbf{S}_{TT}}^{-1}\mathbf{S}_{TN} \\ {\mathbf{C}_{NN}}^{-1}\mathbf{C}_{NT} & {\mathbf{C}_{NN}}^{-1} \end{pmatrix} \begin{pmatrix} \epsilon_T \\ \sigma_N \end{pmatrix} , \begin{pmatrix} \sigma_T \\ \epsilon_N \end{pmatrix} = \begin{pmatrix} \mathbf{X}_{TT} & \mathbf{X}_{TN} \\ \mathbf{X}_{NT} & \mathbf{X}_{NN} \end{pmatrix} \begin{pmatrix} \epsilon_T \\ \sigma_N \end{pmatrix} \qquad (\mathrm{A}-7.5)$$

With the above rearrangement of tensor components one has reached the group domain representation for a horizontally layered earth. It relates continuous quantities σ_N and ϵ_T with discontinuous quantities σ_T and ϵ_N across layer interfaces. The Conversion of the group domain back to the original stiffness or compliance representation simply repartitions stresses, strains, and hybrid matrix X to their conventional form.

7.7.3 Applying averaging operators in the group domain

In the group domain representation I replace the layered overburden with a homogeneous medium such that the total displacement of the top of the stack is given by the integral of the normal strains over the thickness of the stack. The total force acting perpendicular to the layering is given by the integral of the tangential stresses over the thickness of the stack. To achieve equivalence one must preserve the integral of the discontinuous components over the thickness of the stack:

$$\int \begin{pmatrix} {\sigma_T}^{equiv} \\ {\epsilon_N}^{equiv} \end{pmatrix} dz = \int \begin{pmatrix} \sigma(z)_T \\ \epsilon(z)_N \end{pmatrix} dz = \int \begin{pmatrix} \mathbf{X}(z)_{TT} & \mathbf{X}(z)_{TN} \\ \mathbf{X}(z)_{NT} & \mathbf{X}(z)_{NN} \end{pmatrix} dz \begin{pmatrix} \epsilon_T \\ \sigma_N \end{pmatrix} \qquad (\mathrm{A}-7.6)$$

Since the normal components of the stresses and the tangential components of the strains are constant within the medium, one can obtain the integrated quantities, by computing

an integral over the material properties with the stresses and stains pulled out of the integral. The homogeneous equivalent medium has constant medium properties, so that

$$\int \begin{pmatrix} {\sigma_T}^{equiv} \\ {\epsilon_N}^{equiv} \end{pmatrix} dz = \int dz \begin{pmatrix} {\mathbf{X}_{TT}}^{equiv} & {\mathbf{X}_{TN}}^{equiv} \\ {\mathbf{X}_{NT}}^{equiv} & {\mathbf{X}_{NN}}^{equiv} \end{pmatrix} \begin{pmatrix} \epsilon_T \\ \sigma_N \end{pmatrix} \qquad (\mathrm{A}-7.7)$$

The replacement medium is then determined by the following relations:

$$\begin{aligned} z^{equiv} &= \int dz \\ \rho^{equiv} &= \frac{1}{z^{equiv}} \int \rho(z) dz \\ \mathbf{X}^{equiv} &= \frac{1}{z^{equiv}} \int \mathbf{X}(z) dz \end{aligned} \qquad \text{(A-7.8)}$$

7.8 Appendix B: Approximating TI media with elliptic coefficients

In this section I show the approximate velocity expressions that I used after the well log was averaged in the group domain and became anisotropic. Although velocity versus propagation angle can be determined exactly, I limit myself to the propagation directions close to the vertical axis (because of the surface seismic experiment) and I can thus use Muir's simplified expressions. Adhering to Muir's notation, I use the following symbols: W_{ij} is $(1/\rho)C_{ij}$, an elastic modulus divided by density; C is $\cos\theta$; S is $\sin\theta$. More detailed and complete definitions for all wave types appear in (Muir, 1991b).

The relations between velocity and elastic properties are summarized here for P-wave propagation only:

$$W_{P,x} = W_{11} \tag{B-7.1}$$

$$W_{P,xnmo} = W_{44} + \frac{(W_{13}+W_{44})^2}{W_{33}-W_{44}} \tag{B-7.2}$$

$$W_{P,z} = W_{33} \tag{B-7.3}$$

$$W_{P,znmo} = W_{44} + \frac{(W_{13}+W_{44})^2}{W_{11}-W_{44}}. \tag{B-7.4}$$

Similar expressions can be found for SV- and SH-waves, if one would like to go beyond the scope of this chapter and estimate more than P-wave velocities from the averaged log.

If the paraxial move-out velocity equals the axial velocity, then the medium will be isotropic in kinematic approximation for the wave type concerned. The condition for this pseudo-isotropy around the Z axis is that

$$W_z \quad = \quad W_{xnmo}. \tag{B-7.5}$$

For P-waves, then,

$$W_{33} \quad = \quad W_{44} + \frac{(W_{13}+W_{44})^2}{W_{33}-W_{44}}, \tag{B-7.6}$$

which determines the condition

$$(W_{13}+W_{44})^2 \quad = \quad (W_{33}-W_{44})^2. \tag{B-7.7}$$

Appendix A

Programming utilities

A.1 RatFor == RATional FORtran

Up to now **Fortran** is our most universal computer language for computational physics. For general programming, however, it has been surpassed by **C**. "**Ratfor**" is Fortran with C-like syntax and combines uncluttered, free-form programming with the power of clearly displaying mathematical formulas and algorithms. Ratfor accepts constructs that are possible in any of the Fortran dialects (Fortran IV, 66, 77, 90 and HPF). As illustrated in chapter 5, I used Ratfor90 to implement an entire tool box of wave equation modules. My choice of Ratfor90 is dictated by the need for computational efficiency of parallel computers (thus Fortran90 or HPF) and the wish to actually include the code of algorithms in this thesis. The Ratfor preprocessor is now, usually included in the Fortran compiler environment, but a public domain version is also available. [1]

A.1.1 General ratfor language features

The following paragraphs are reprinted from Jon Claerbout's Ratfor feature summary, published in *Earth Sounding Analysis: Processing versus Inversion* (1992) and *Applications of Three Dimensional Filtering* (1994):

> Ratfor was invented by the people who invented C. Ratfor programs are converted to Fortran with the Ratfor **preprocessor**. Since the preprocessor is publicly available, Ratfor is practically as universal as Fortran. [Ratfor was

[1] `available from http://sepwww.stanford.edu/sep/prof`

invented at AT&T (Kernighan, 1976), which makes it available directly or through many computer vendors. The original Ratfor transforms Ratfor code to **Fortran** 66. See `http://sepwww.stanford.edu/sep/prof` for a general public-domain Ratfor translator.]

You will not really need the Ratfor preprocessor or any precise definitions if you already know Fortran or almost any other computer language, because then the Ratfor language will be easy to understand. Statements on a line may be separated by ";". Statements may be grouped together with braces { }. `Do` loops do not require statement numbers because { } defines the range. Given that `if( )` is true, the statements in the following { } are done. `else`{ } does what you expect. We may *not* contract `else if` to `elseif`. We may always omit the braces { } when they contain only one statement. `break` will cause premature termination of the enclosing { }. `break 2` escapes from {{ }}. `while( )` { } repeats the statements in { } while the condition ( ) is true. `repeat` { `...` } `until( )` is a loop that tests at the bottom. A looping statement more general than `do` is `for(initialize; condition; reinitialize)` { }. An example of one equivalent to `do i=0,n-1` is the looping statement `for(i=0;i<n;i=i+i)`. The statement `next` causes skipping to the end of any loop and a retrial of the test condition. `next` is rarely used, but when it is, we must beware of an inconsistency between Fortran and C-language. Where Ratfor uses `next`, the C-language uses `continue` (which in Ratfor and Fortran is merely a place holder for labels).

The Fortran relational operators `.gt.`, `.ge.`, `.ne.`, etc. may be written >, >=, !=, etc. The logical operators `.and.` and `.or.` may be written & and |. Anything from a # to the end of the line is a comment. Anything that does not make sense to the Ratfor preprocessor, such as Fortran input-output, is passed through without change.

Ratfor has an `include` statement, which includes the specified filename. In the source code abbreviations are possible by using the `define` statement. As Claerbout describes:

> Indentation in `Ratfor` is used for readability. It is not part of the `Ratfor` language. One may choose one's own style.

A.2 SPP – A general CPP like preprocessor

CPP is the standard preprocessor that accompanies any C compiler and is designed to work on directives in the C language. It recognizes the symbols `/* */` as comments and the symbol # as preprocessor directive. It is a powerful tool in writing clean and general code.

Similar preprocessors exist for other languages, such as Fortran, but I found many vendor dependent inconsistencies. Since I wanted to design a portable code tool box, I decided to write my own preprocessor **SPP** whose features include those of CPP, and which would perform identically on any machine. I implemented it in the "Perl" language, which is a superset of `awk, grep, sed and C` and a powerful tool. Perl is public domain and available on most computers.

The basic feature of SPP [1] is the specification of an arbitrary comment symbol and directive symbol. Its syntax and features also include those of CPP. Following is the manual page that accompanies SPP.

```
CPP(1)                    USER COMMANDS                    CPP(1)
NAME
      spp - SEP's ANY language preprocessor

 SYNOPSIS
      spp [ -Ccommentsymbols ] [ -strict ] [  -f77  ]  [  -H  ]  [ -undef ]
           [ -Dname ] [ -Dname=def ] [ -Idirectory ] [ -Uname ]
           [ -Ydirectory ] [ <input-file [ >output-file ] ]

 DESCRIPTION
      spp is the ANY language language preprocessor.
      SPP is a preprocessor that differs from CPP only in that
      specficiation of arbitrary comment and directive symbols
      are possible (e.g., %#$define, instead of #define).
      So it can be used for many different programming languages.
      Although spp can be used as a macro processor, this  is  not
      normally  recommended. For general-purpose macro-processing,
      see m4(1V), and the chapter on m4 in  Programming  Utilities
      and Libraries.
      spp  redirects  standard  in  and  out.    <input-file   and
      >output-file


 OPTIONS
      -C   Define what the comment symbol is (# for ratfor, c  for
           f77  etc)  that  contains  spp directive lines. In this
           manual page  the  the  usual  #  directive  symbols  is
           assumed   to  epxlain  the  syntax  and  features.   By
           default, spp leaves in all commment lines.
      -strict
           Forces comment symbol and processor  directives  to  be
           adjacent (like #ifdef), then all lines like (#   ifdef)
           are treated as comments.
      -f77 Run the preprocessor in Fortran 77 mode,  it  correctly
           handles lines longer than 72 columns....
```

[1] SPP is available from ftp://sepftp.stanford.edu/pub/SPP

Bibliography

Aki, K., and Richards, P., 1980, Quantitative seismology theory and methods I: Freeman.

Al, K., 1989, Velocity analysis by iterative profile migration: Geophysics, **54**, no. 6, 718–729.

Alford, R. M., 1986, Shear data in the presence of azimuthal anisotropy: Dilley, texas: 56th Annual Internat. Mtg., Soc. Expl. Geophys., Expanded Abstracts, Session:S9.6.

Auld, B. A., 1973, Acoustic fields and waves in solids: John Wiley & Sons.

Backus, G. E., 1962, Long-wave anisotropy produced by horizontal layering: J. Geophys. Res., **66**, 4427–4440.

Baeten, G. J. M., Fokkema, J. T., and Ziolkowski, A. M., 1989, Feedback signal of a seismic vibrator: 59th Annual Internat. Mtg., Soc. Expl. Geophys., Expanded Abstracts, 680.

Biot, M. A., 1965, Mechanics of incremental deformations: John Wiley & Sons.

Bishop, G. W., 1989, Amplitude controls in the Pembrook multi-component surface data: Technical Abstract, SEG Workshop on Recording and Processing Vector Wave Field Data.

Carrion, P. M., Sacramento, S. S., and Pestana, C. R., 1990, Source wavelet and its angular spectrum from plane-wave seismograms: Geophysics, **55**, no. 8, 1026–1035.

Claerbout, J. F., 1986, Simultaneous pre-normal moveout and post-normal moveout deconvolution: Geophysics, **51**, no. 7, 1341–1354.

Claerbout, J. F., 1992, Earth Soundings Analysis: Processing versus Inversion: Blackwell Scientific Publications.

Claerbout, J. F., 1994, Applications of three-dimensional filtering: SEP.

Cunha, C., 1991, Angle dependent reflectivity from elastic reverse time migration: SEP–**72**, 111–122.

Dablain, M. A., 1986, The application of high-order differencing to the scalar wave equation: Geophysics, **51**, no. 1, 54–66.

Dellinger, J., and Muir, F., 1986, NMO and beating the central limit theorem: SEP–**48**, 261–268.

Dellinger, J., and Muir, F., 1993, Dix revisited: a formalism for rays in layered media: Fifth international workshop on seismic anisotropy, Canadian Soc. Expl. Geophys., Proceedings of the Fifth International Workshop on Seismic Anisotropy.

Dellinger, J., Muir, F., and Karrenbach, M., 1993, Anelliptic approximations for TI media: Journal of Seismic Exploration, **2**, 23–40.

Dellinger, J., 1991, Anisotropic seismic wave propagation: SEP–**69**, 0.

Duong-van, M., 1992 Workshop on Chaos at Lawrence Livermore National Laboratory, pers. comm.

Emerman, S. H., Schmidt, W., and Stephen, R. A., 1982, An implicit finite-difference formulation of the elastic wave equation: Geophysics, **47**, no. 11, 1521–1526.

Etgen, J., 1989, Accurate wave equation modeling: SEP–**60**, 131–148.

Feit, M., 1992 Workshop on Chaos at Lawrence Livermore National Laboratory, pers. comm.

Fenati, D., and Rocca, F., 1984, Seismic reciprocity field tests from the Italian Peninsula: Geophysics, **49**, no. 10, 1690–1700.

Filho, C. A. C., 1992a, Elastic modeling and migration in earth models: Ph.D. thesis, Stanford University.

——— 1992b, Elastic modeling in discontinuous media: Testing the dynamic response: SEP–**73**, 317–330.

Fokkema, J. T., Baeten, G. J. M., and Vaage, S., 1990, Directional deconvolution in the f-x domain: 60th Annual Internat. Mtg., Soc. Expl. Geophys., Expanded Abstracts, 1673–1676.

Folstad, P. G., and Schoenberg, M., 1992, Use of equivalent anisotropic medium theory to calculate synthetic seismograms: SEG Summer Research Workshop on AVO, Soc. Expl. Geophys., Expanded Abstracts.

Fung, Y., 1965, Foundations of solid mechanics: Prentice-Hall, Inc.

Gangi, A. F., 1980, Theoretical basis of seismic reciprocity: 50th Annual Internat. Mtg., Soc. Expl. Geophys., Reprints, Session:SR.1.

Gibson, B., and Larner, K., 1984, Predictive deconvolution and the zero-phase source: Geophysics, **49**, no. 4, 379–397.

Hill, R., 1983, Interfacial operators in the mechanics of composite media: J. Mech. Phys. Solids, **31**, no. 4, 347–357.

Holberg, O., 1987, Computational aspects of the choice of operator and sampling interval for numerical differentiation in large-scale simulation of wave phenomena: Geophys. Prosp., **35**, no. 6, 629–655.

Holberg, O., 1988, Towards optimum one-way wave propagation: Geophys. Prosp., **36**, no. 2, 99–114.

Igel, H., Riollet, B., and Mora, P., 1992, Accuracy of staggered 3-d finite-difference grids for anisotropic wave propagation: Annual International SEG meeting 1992, Soc. Expl. Geophys., Expanded Abstracts, 1244–1246.

Karrenbach, M., Muir, F., and Nichols, D., 1992, Modeling reflections from the Austin Chalk – a practical application of azimuthal anisotropy: SEG Summer Research Workshop on AVO, Soc. Expl. Geophys., Expanded Abstracts, 622–622.

Karrenbach, M., 1991, Prestack reverse time migration in anisotropic media: SEP–**70**, 113–122.

Keho, T. H., Weglein, A. B., and Rigsby, P. G., 1990, Marine source wavelet and radiation pattern estimation: 60th Annual Internat. Mtg., Soc. Expl. Geophys., Expanded Abstracts, 1655–1657.

Kennett, B. L. N., 1974, Reflections, rays and reverberations: BSSA, **64**, 1685–1696.

Kerley, L. M., 1988, Comprehending the Central Limit Theorem: SIGCSE Bulletin, **20**, no. 2, 20–25.

Kernighan, B. W., 1976, Software tools: Addison-Wesley.

Kjartansson, E., 1979, Attenuation of seismic waves in rocks and applications in energy exploration: Ph.D. thesis, Stanford University.

Knopoff, L., and Gangi, A. F., 1959, Seismic reciprocity: Geophysics, **24**, no. 4, 681–691.

Kosik, D. W., 1993, Propagation of a nonlinear seismic pulse in an anelastic homogeneous medium: Geophysics, **58**, no. 7, 949–963.

Levin, S., 1987, Deconvolution with spatial constraints: Ph.D. thesis, Stanford University.

Mikhailenko, B., 1991, personal communication:.

Mora, P., 1987, Elastic wavefield inversion: Ph.D. thesis, Stanford University.

Morse, P. M., and Feshbach, H., 1953a, Methods of theoretical physics:, volume II McGraw-Hill Book Company, Inc.

——— 1953b, Methods of theoretical physics I: McGraw-Hill Book Company, Inc.

Muir, F., 1991a, Experience with Connection Machine Fortran: SEP–**70**, 53–58.

——— 1991b, Various equations for transverse isotropic media: SEP–**70**, 367–372.

Newell, C., 1974, Nonlinear wave motion: American Mathematical Society.

Nichols, D., and Karrenbach, M., 1990, What is equivalent in an equivalent medium ?: SEP–**67**, 1–4.

Nichols, D., Urdaneta, H., Oh, H. I., Claerbout, J., Laane, L., Karrenbach, M., and Schwab, M., 1993, Programming geophysics in C++: SEP–**79**, 313–471.

Nichols, D., 1989, Converting surface motions to subsurface wavefields: SEP–**61**, 179–200.

Nichols, D., 1991, A simple wave filed separation scheme: SEP–**72**, 195–212.

Pao, Y.-H., and Varatharajulu, V., 1976, Huygens' principle, radiation conditions, and integral formulas for the scattering of elastic waves: J. Acoust. Soc. Am., **59**, no. 6, 1361–1371.

Razavy, M., and Lenoachca, B., 1986, Reciprocity principle and the approximate solution of the wave equation: Bulletin of the Seismological Society of America, **76**, no. 6, 1776–1789.

Roberts, G. A., and Goulty, N. R., 1990, Directional deconvolution of marine seismic reflection data: North sea example: Geophys. Prosp., **38**, no. 8, 881–888.

Ronen, J., and Claerbout, J. F., 1985, Surface-consistent residual statics estimation by stack-power maximization: Geophysics, **50**, no. 12, 2759–2767.

Schoenberg, M., and Muir, F., 1989, A calculus for finely layered anisotropic media: Geophysics, **54**, no. 5, 581–589.

Shuey, R. T., 1985, A simplification of the Zoeppritz-Equations: Geophysics, **50**, no. 4, 609–614.

Stam, H. J., 1990, The two-dimensional elastodynamic distributed surface load problem: Geophysics, **55**, no. 8, 1047–1056.

Summer Research Workshop, S., 1989, Technical abstracts: SEG workshop on recording and processing vector wave field data: Society of Exploration Geophysicists.

Tarantola, A., 1987, Inverse problems theory: Elsevier.

Toldi, J., 1985, Velocity analysis without picking: Ph.D. thesis, Stanford University.

Versteeg, R., and Grau, G., 1990, Practical aspects of seismic data inversion, the Marmousi experience: 52nd EAEG Meeting, Eur. Assoc. Expl. Geophys., Proceedings of 1990 EAEG Workshop, 1–194.

Virieux, J., 1986, P-SV wave propagation in heterogeneous media - velocity-stress finite-difference method: Geophysics, **51**, no. 4, 889–901.

Walker, D. A., 1993, Harmonic resonance structure and chaotic dynamics in the land vibrator system: 55th Meeting and Technical Exhibition - Stavanger, European Assoc. Expl. Geophys., Expanded Abstracts.

Weglein, A. B., and Secrest, B. G., 1990, Wavelet estimation for a multidimensional acoustic or elastic earth: Geophysics, **55**, no. 7, 902–913.

Whitham, G. B., 1974, Linear and nonlinear waves: John Wiley & Sons.

Wiggins, R. A., Larner, K. L., and Wisecup, R. D., 1976, Residual static analysis as a general linear inverse problem: Geophysics, **41**, no. 5, 922–938.

Yurinskii, V. V., 1977, On the error of the Gaussian approximation for convolutions: Theory Probab. Appl., **22**, 236–247.

Zoeppritz, K., 1919, Ueber die Erdbebenwellen: Goettinger Nachrichten der Koenigl. Gesells. Wissen., pages 66–84.

Index